



# Microstructural and corrosion characteristics of tantalum coatings prepared by molten salt electrodeposition<sup>☆</sup>

Y.J. Lee<sup>a</sup>, T.H. Lee<sup>b</sup>, D.Y. Kim<sup>a</sup>, H.H. Nersisyan<sup>b</sup>, M.H. Han<sup>a</sup>, K.S. Kang<sup>c</sup>, K.K. Bae<sup>c,\*\*</sup>, Y.J. Shin<sup>d</sup>, J.H. Lee<sup>b,\*</sup>

<sup>a</sup> Graduate School of Green Energy Technology, Chungnam National University, Daejeon 305-764, Republic of Korea

<sup>b</sup> Graduate School of Department of Metallurgical Engineering, Chungnam National University, Daejeon 305-764, Republic of Korea

<sup>c</sup> Korea Institute of Energy Research, 152 Gajeong-ro, Yuseong-gu, Daejeon 305-343, Republic of Korea

<sup>d</sup> Korea Atomic Energy Research Institute, 1045 Daedeok-daero, Yuseong-gu, Daejeon 305-353, Republic of Korea

## ARTICLE INFO

### Article history:

Received 19 March 2013

Accepted in revised form 5 September 2013

Available online 12 September 2013

### Keywords:

Molten salt

Electroplating

Tantalum

Corrosion resistance

Coating layer

## ABSTRACT

A study has been conducted on the electrodeposition of tantalum in a 61 mol% LiF–39 mol% NaF melt containing 1 mol% K<sub>2</sub>TaF<sub>7</sub> at 800 °C. Tantalum was coated onto a stainless-steel base (SUS316L) by molten salt electrodeposition (MSE) at different current densities (0.5, 1.5, 2, 5, 10, 20 mA/cm<sup>2</sup>). Electrodeposition of metallic tantalum occurred primarily by electroreduction of Ta(V), i.e. TaF<sub>2</sub><sup>+</sup>, at a potential of <−0.27 V (vs. Pt used as a pseudo reference electrode). At potentials less than −0.324 V, TaF<sub>2</sub>(s) also underwent reduction to metallic tantalum. Pure metallic tantalum, without any entrapped salt, was successfully deposited on SUS316L by electrodeposition at 5 mA/cm<sup>2</sup>. This showed that the deposition efficiency and microstructure of the tantalum coating layer were strongly dependent on the current density. The densest microstructure was obtained at a current density of 5 mA/cm<sup>2</sup>. Current densities above 5 mA/cm<sup>2</sup> caused non-uniform microstructures because of rapid deposition. A dense microstructure and an intact coating layer contributed to a significant enhancement in corrosion resistance.

© 2013 The Authors. Published by Elsevier B.V. All rights reserved.

## 1. Introduction

The corrosion resistance and basic physical properties of solid tantalum are not comparable to most structural metallic materials. Particularly, in the case of the sulfur–iodine (SI) cycle combined with a very high temperature gas-cooled reactor (VHTR), wherein a chemical reaction between H<sub>2</sub>SO<sub>4</sub> and HI occurs at temperatures greater than 300 °C and pressures of 2–3 MPa, the structural material related to the SI process may undergo severe corrosion. The relatively high cost and melting temperature of tantalum present obstacles to its widespread application in general engineering processes. The most interesting characteristics of tantalum are its surface corrosion resistance properties. For instance, the amorphous and nanocrystalline valve-metal alloy coatings exhibit extremely high corrosion resistance in concentrated HCl. These can be used to advantage by employing a tantalum coating on a base metal or alloy that best fits with the engineering requirements in a cost-

effective manner. It has already been reported by Senderoff et al. [1] that electrodeposition in molten salt facilitates the coating of metallic tantalum. Molten salt electrodeposition (MSE) processes for tantalum were reviewed by Cardarelli et al. and compared with other coating techniques [2]. The main advantages of MSE are accurate controllability of the coating thickness, simplicity of operation, high deposition rate, and good throwing power. There are various reports on fundamental electrochemical studies [3] and the formation of dense, uniform tantalum and alloy coating layers on different substrates [4–7]. Recent studies on electrodeposition at room temperature in ionic liquids show that metallic tantalum could be coated onto metal substrates [8–10]. However, the optimum conditions for obtaining a dense and coherent tantalum coating layer are stringent, and flaking or cracking defects occur under certain conditions during electrodeposition. Furthermore, no systematic study on the effects of processing parameters on the microstructure formation of tantalum and its corrosion characteristics in high-temperature HI solution has yet been reported. A good coating of pure tantalum may enhance its industrial applications in severely corrosive environments. In this study, we focused on the microstructure evolution of the tantalum coating layer to understand the effects of processing parameters on coating qualities such as density, surface roughness, and hardness. The coated specimens prepared at different current densities were subjected to a corrosion test in high-pressure and high-temperature HI solution.

<sup>☆</sup> This is an open-access article distributed under the terms of the Creative Commons Attribution-NonCommercial-No Derivative Works License, which permits non-commercial use, distribution, and reproduction in any medium, provided the original author and source are credited.

\* Corresponding author. Tel.: +82 42 821 6596; fax: +82 42 822 5850.

\*\* Corresponding author:

E-mail addresses: [kkbae@kier.re.kr](mailto:kkbae@kier.re.kr) (K.K. Bae), [jonglee@cnu.ac.kr](mailto:jonglee@cnu.ac.kr) (J.H. Lee).

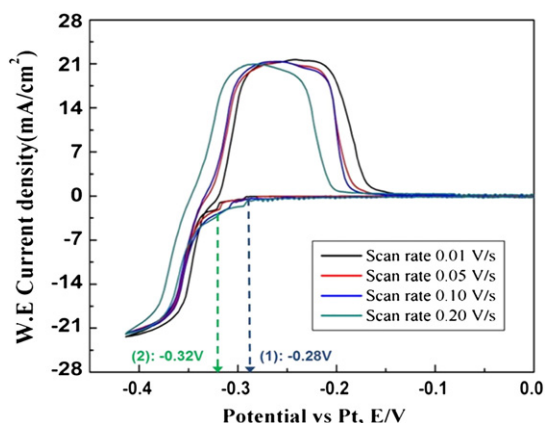


Fig. 1. Cyclic voltammograms obtained with Pt at different sweep rates. The electrolyte was a LiF–NaF melt containing 1 mol%  $K_2TaF_7$ .

**Table 1**  
Calculated electrodeposition time for uniform coating thickness.

Current density (mA/cm <sup>2</sup> )	Operating time (h)	Calculated coating thickness (μm)	Measured coating thickness (μm)
0.5	74.16	30	9.07 ± 6.12
1.5	24.72	30	17.15 ± 8.63
2	18.54	30	15.12 ± 3.62
5	7.41	30	30.21 ± 1.09
10	3.70	30	14.95 ± 3.71
20	1.85	30	10.46 ± 7.34

## 2. Material and methods

Analytical-grade LiF, NaF, and  $K_2TaF_7$  were purchased from Wako Pure Chemical (Osaka, Japan). The purity of all chemicals was 99.9%, and the chemicals were used after drying at 300 °C for 24 h.

The substrate specimens used were 40 mm × 20 mm × 2 mm commercial stainless steel plates. Its chemical composition is as follows: Cr 18%, Ni 2.5%, Mo 3.5%, C 0.080% and Fe balance. These plates were polished with 1500-grit SiC paper and then cleaned ultrasonically in acetone.

The cell consisted of a nickel crucible, a tantalum plate as the counter electrode, a platinum wire as the reference electrode (and working electrode for cyclic voltammetry (CV) experiments), and an SUS316 plate as the working electrode for chronopotentiometry (CP) experiments. A

vertical Inconel 625 tube was used as the reaction chamber. The temperature of the chamber was measured using an R-type thermocouple. The temperature was controlled within 0.5 K by a thermostat, and the molten salt was stirred throughout the experiment, except in the CV experiments. LiF, NaF, and  $K_2TaF_7$  were mixed by direct weighing in a molar ratio of 60.4:38.6:1. The crucible containing the salt mixture was placed in the chamber, and then, the chamber temperature was raised to 800 °C. All experiments were performed in an Ar glove box, which was maintained at oxygen and moisture concentrations below 10 ppm, because of the high reactivity of tantalum ions with oxygen [11]. After the electrodeposition of tantalum, the specimens were withdrawn from the molten salt and cooled to room temperature. The adhered molten salt was washed off by ultrasonic treatment in 20% HCl solution for 5 h, and the specimen was dried.

The electrochemical measurements were performed with the help of a potentiostat (AUT70530, Utrecht, Netherlands). Ta deposition layer thickness and morphology with experimental conditions were measured by using the field-emission scanning electron microscopy (FE-SEM, JSM 6330F, Japan). The tantalum coating layers were characterized by X-ray diffraction (XRD, Siemens D5000, Germany), field-emission scanning electron microscopy, energy-dispersive X-ray (EDX, JSM 5410, Japan) analysis, orientation imaging microscopy (OIM, JSM 5410, Japan), atomic force microscopy (AFM, NanoScope V, Japan) and micro Vickers hardness testing (FM-7, Future Tech Co., Ltd., Japan). Furthermore, corrosion tests were conducted in autoclave systems (100 h, 150 °C, 2 MPa, HI = 26.1, I<sub>2</sub> = 51.8, H<sub>2</sub>O = 22.0 wt.%).

## 3. Results and discussion

Fluoride melts (LiF–NaF) were used in the experiments to avoid disproportionation reactions, which hinder coherent deposition of tantalum [12]. The characteristics of the fluoride-based molten salt are very favorable for achieving coherent, dense, and adherent tantalum deposits onto the base metal. In the melt, tantalum existed as a complex species,  $TaF_7^{2-}$ . The tantalum salt used as a solute in the melt could be tantalum pentafluoride ( $TaF_5$ ) or potassium heptafluorotantalate ( $K_2TaF_7$ ). The mechanism of electrochemical reduction of Ta(V) in these melts has been previously reported: a detailed discussion of tantalum reduction in fluoride melts has been reviewed by Polyakova et al. [13]. Senderoff et al. have shown that in a fluoride melt at 800 °C, reduction occurs in two steps, as follows [1]:

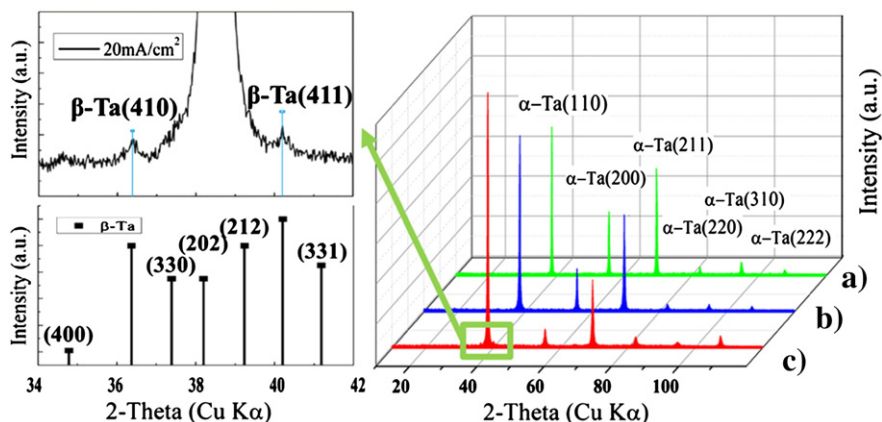
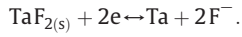


Fig. 2. Typical XRD patterns obtained from tantalum coatings prepared in LiF–NaF melts containing 1 mol%  $K_2TaF_7$  at different current densities: a) 1.5 mA/cm<sup>2</sup>; b) 5 mA/cm<sup>2</sup>; c) 20 mA/cm<sup>2</sup>.



(2)

In order to verify the electrode reactions shown in Eqs. (1) and (2) in this molten salt system containing 1 mol%  $\text{K}_2\text{TaF}_7$ , cyclic voltammograms were recorded at sweep rates from 0.01 to 0.2 V/s. Fig. 1 shows a cyclic voltammogram obtained with a Pt working electrode, in the LiF–NaF

melt containing 1 mol%  $\text{K}_2\text{TaF}_7$ . The voltammogram shows two distinct waves related to the electroreduction of fluorotantalate to metallic tantalum. The first reaction is the reduction of  $\text{TaF}_7^{2-}$  to  $\text{TaF}_2$  with a charge transfer number of 3. This reaction occurs at  $-0.28$  to  $-0.32$  V vs. Pt in the melt containing 1%  $\text{K}_2\text{TaF}_7$ . The second reduction is the electrodeposition of metallic tantalum from  $\text{TaF}_2$  with a charge transfer number of 2 at  $-0.32$  V.

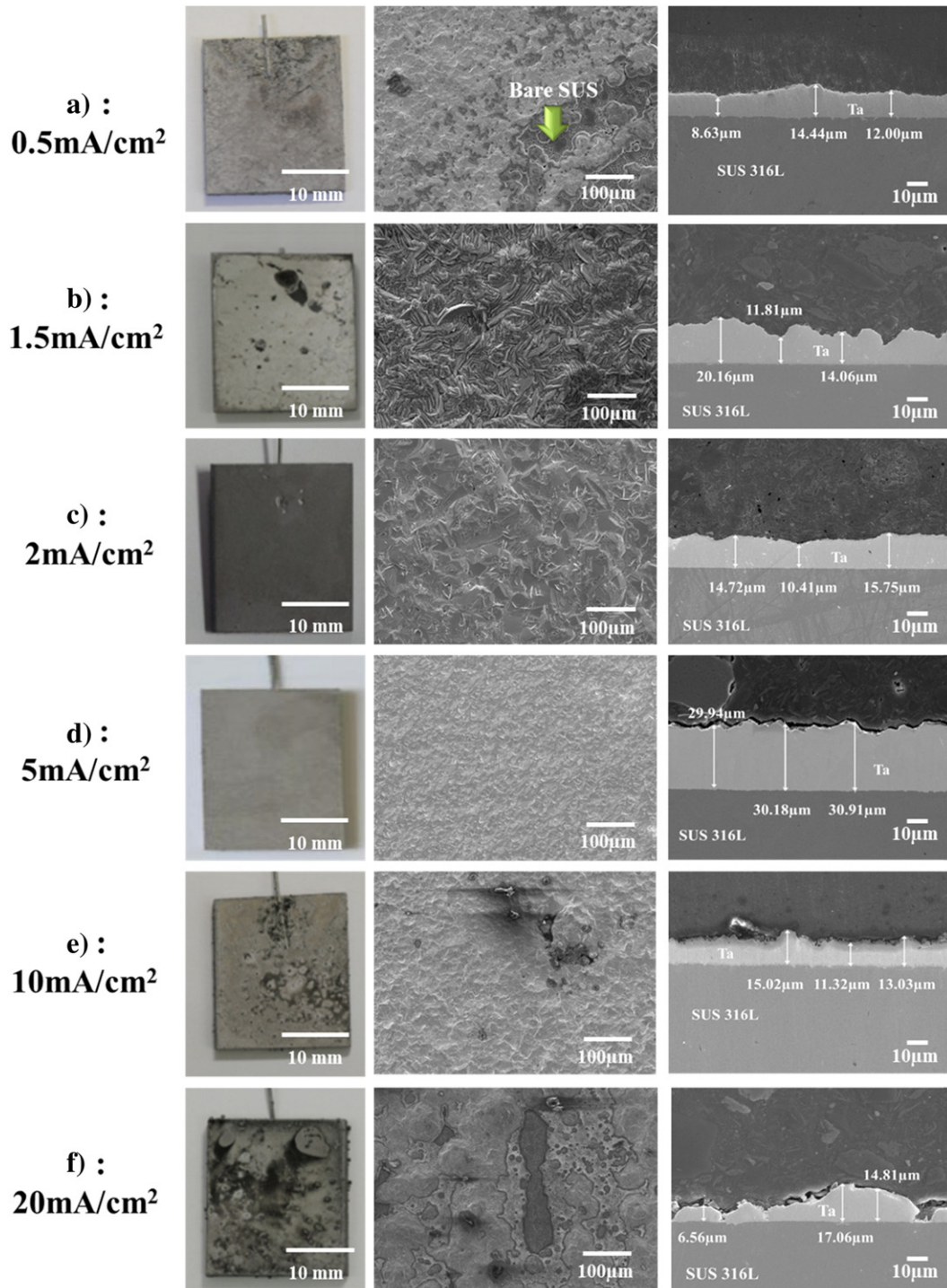


**Fig. 3.** SEM micrographs of the surfaces and cross-sections of tantalum deposits on SUS316L according to applied current density: a) 0.5 mA/cm<sup>2</sup>; b) 1.5 mA/cm<sup>2</sup>; c) 2 mA/cm<sup>2</sup>; d) 5 mA/cm<sup>2</sup>; e) 10 mA/cm<sup>2</sup>; f) 20 mA/cm<sup>2</sup>.

The operating time to form a 30- $\mu\text{m}$ -thick coating layer on the base metal (SUS316L) substrate can be estimated by using Eq. (3):

$$T_{(s)} = C_g / \left( W_{eq} \times C_A \right), \quad C_g = A \times \rho \times C_t \quad (3)$$

where  $T_{(s)}$  is the operating time for obtaining the target coating thickness,  $W_{eq}$  is the electrochemical equivalent of tantalum,  $C_A$  is the current applied to the electrode,  $A$  is the area of SUS316L,  $\rho$  is the density of tantalum,  $C_t$  is the target coating thickness, and  $C_g$  is the surface coating mass of tantalum for SUS316 electrodeposition. The calculated operating times are shown in Table 1.

Fig. 2 depicts the XRD patterns of the tantalum coating layers prepared in the molten salt (LiF–NaF) melt containing 1 mol%  $\text{K}_2\text{TaF}_7$  for different current densities. It is well known that tantalum coating layers have two distinct phases,  $\alpha$  and  $\beta$ . In all cases, the XRD peaks detected at  $38.72^\circ$ ,  $56.21^\circ$ ,  $69.7^\circ$ ,  $81.19^\circ$ ,  $94.4^\circ$ , and  $107.7^\circ$  related to  $\alpha$ -Ta (1 1 0), (2 0 0), (2 1 1), (2 2 0), (3 1 0), and (2 2 2), respectively [14]. In the particular case of a current density of  $20 \text{ mA/cm}^2$ , the XRD peaks detected at  $36.28^\circ$  and  $40.2^\circ$  related to  $\beta$ -Ta (4 1 0) and (4 1 1), respectively.  $\beta$ -Ta is a metastable phase, which transforms to  $\alpha$ -Ta when heated to temperatures between  $750$  and  $900^\circ\text{C}$  [15]. However, for the current density of  $20 \text{ mA/cm}^2$ , some residual  $\beta$ -Ta phase remained because of the insufficient process time for

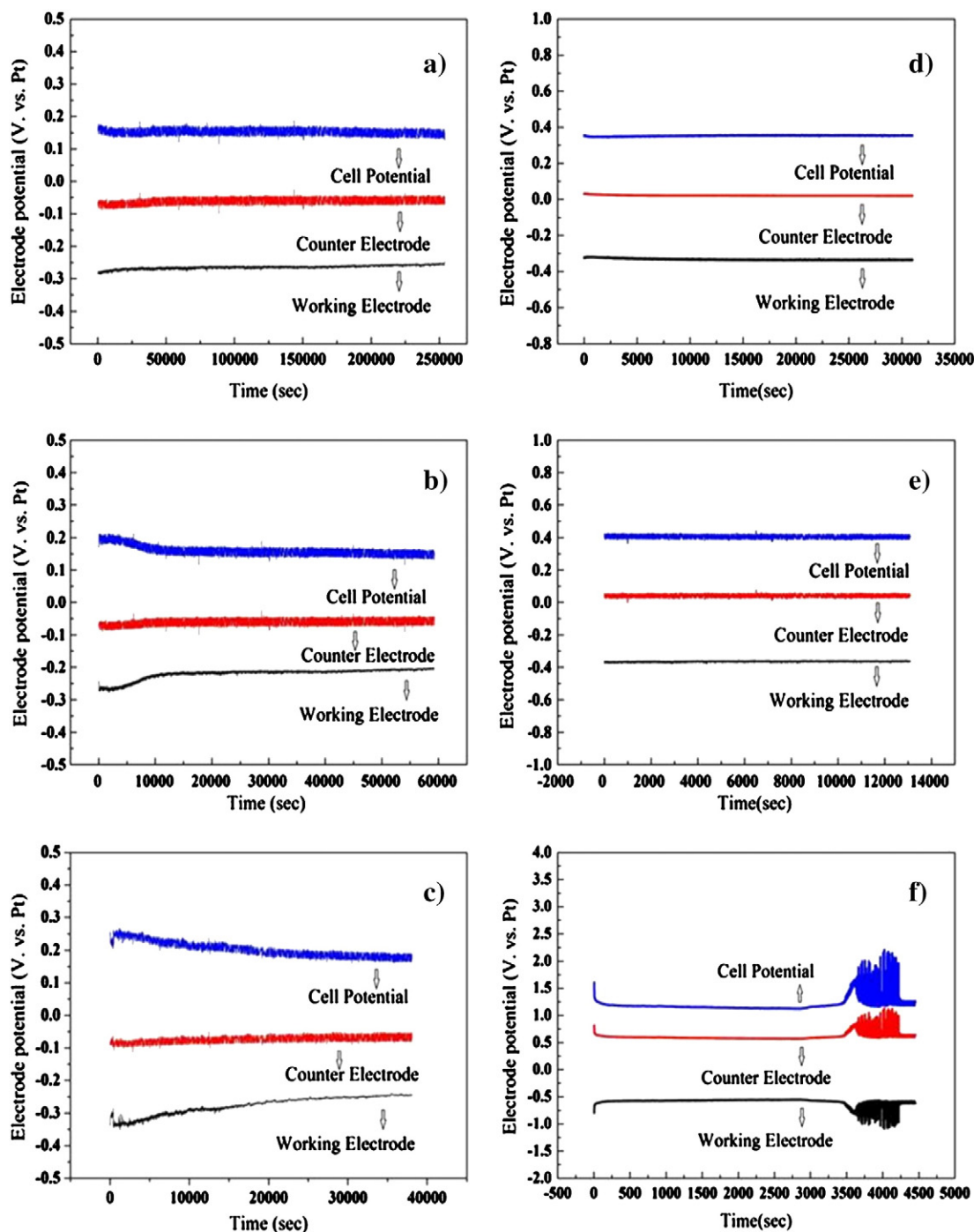


Fig. 4. Chronopotentiometry analysis of tantalum coating in a LiF–NaF melt containing 1 mol%  $\text{K}_2\text{TaF}_7$  at  $850^\circ\text{C}$ , at different applied current densities: a)  $0.5 \text{ mA/cm}^2$ ; b)  $1.5 \text{ mA/cm}^2$ ; c)  $2 \text{ mA/cm}^2$ ; d)  $5 \text{ mA/cm}^2$ ; e)  $10 \text{ mA/cm}^2$ ; f)  $20 \text{ mA/cm}^2$ .

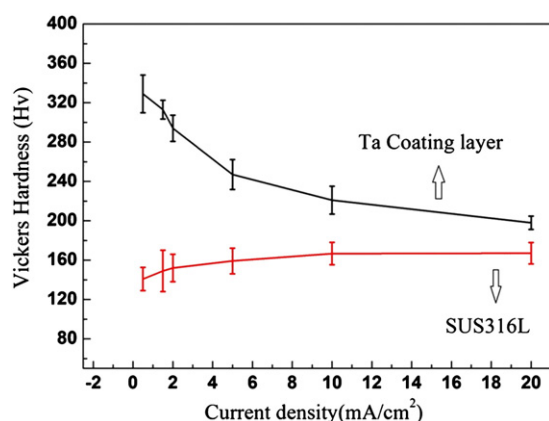


Fig. 5. Variation in micro Vickers hardness of tantalum coatings and SUS316L substrates with applied current density.

transformation to the  $\alpha$ -Ta phase. This is because the total deposition time at 20 mA/cm<sup>2</sup>, 1.85 h, was much shorter than that at 1.5 and 5 mA/cm<sup>2</sup> (24.72 h and 7.41 h, respectively). The  $\alpha$ -Ta phase has excellent chemical, thermal, and mechanical properties, ductility, formability, and corrosion resistance to aggressive hot propellant gases [16–18], while the  $\beta$ -Ta phase is hard, brittle, and thermally unstable. The residual  $\beta$ -Ta phase in the Ta coating layer is expected to adversely affect its corrosion resistance and mechanical properties.

Fig. 3 shows the morphology of the tantalum coating layers obtained at different current densities. At 0.5 and 1.5 mA/cm<sup>2</sup>, non-uniform microstructures and coating thicknesses were obtained even though the same amount of electric current was applied, as shown in Fig. 3a) and b). The corresponding macroscopic photographs also show areas of uncoated SUS substrate (see arrow in Fig. 3a)). These may be caused by an insufficiency of overvoltage for the reduction to metallic tantalum. As the current density increased to 2 mA/cm<sup>2</sup>, the surface morphology significantly improved and there were no uncoated areas, as shown in Fig. 3c). However, the thickness of the tantalum layers ranged from 12.41 to 15.75  $\mu$ m, which was still far from the expected value of 30  $\mu$ m. At 5 mA/cm<sup>2</sup>, a metallic surface with a typical tantalum color was obtained, as shown in Fig. 3 d), and the microstructures of the surface and cross section were smooth and dense, respectively. It should be noted that the coating layer thickness ranged from 29.94 to 31.31  $\mu$ m, close to the designed thickness of 30  $\mu$ m. When the current density was increased to 10 and 20 mA/cm<sup>2</sup>, the quality of the coating layer degraded (see Fig. 3e) and f)). The tantalum layer coated at a current density above 10 mA/cm<sup>2</sup> was so porous that a part of

the layer was exfoliated during the washing of the adhered salt. This was due to concentration polarization, with rapid deposition entrapping the salt in the coating layer during dendritic tantalum growth.

Fig. 4 shows the CP results during tantalum coating according to the applied current density. Uniform potentials were maintained throughout the electrodeposition process except at the highest current density of 20 mA/cm<sup>2</sup>. At 0.5, 1.5, and 2 mA/cm<sup>2</sup>, the electrode potentials of the working electrode were slightly higher than  $-0.324$  V (vs. Pt), the reduction potential of the tantalum ion, as measured from Fig. 1. Hence, insufficient overpotential seems to be the main reason for the coating layer thickness being lower than the designed value shown in Table 1. The electrode potential decreased below  $-0.324$  V (vs. Pt) at 5 mA/cm<sup>2</sup>, as shown in Fig. 4d). Cell potentials of 0.38 V and 0.41 V were stably maintained throughout the electrodeposition at current densities of 5 mA/cm<sup>2</sup> and 10 mA/cm<sup>2</sup> (Fig. 4e)), respectively, whereas severe fluctuation of the electrode potential was observed at 20 mA/cm<sup>2</sup>, as shown in Fig. 4f). From the poor quality of the tantalum coating layer obtained at 20 mA/cm<sup>2</sup> (Fig. 3f)), the fluctuation seems to be closely related to the concentration overpotential.

The hardness test was carried out to measure the hardness of both SUS316L and the tantalum coating layer. The data are summarized in Fig. 5. The bars indicate the variation in hardness across the specimens. From the hardness variation, it is apparent that the density of the tantalum coating layers decreases with increasing current density. The mechanical properties of the coating layer also seem to be closely related to the microstructural change associated with current density. Hence, dendritic growth of a low-density coating layer may contribute to a decrease in hardness. The hardness decrease in the case of the SUS316L substrate can be explained by annealing during the coating, with the specimens at low current densities being exposed for longer times at the operational temperature of 800 °C. From the fact that the initial hardness of the SUS316L substrate was 176 Hv, the decrease with coating time range from 5.1% (167 Hv) to 20.3% (140.8 Hv) should not present a serious problem for ordinary applications requiring corrosion resistance.

Fig. 6 shows the cross-section of the coated electrode at 5 mA/cm<sup>2</sup>. The intermetallic compound (IMC) layer, observed at the interface between tantalum and the SUS316L substrate, grows significantly during deposition of pure tantalum, because of the diffusion of tantalum atoms inward and iron atoms outward. The IMC thickness increased to about 0.21  $\mu$ m. EDX was carried out at point A for the concentration analysis of the components. As expected, 85.93 wt.% tantalum and 14.07 wt.% iron were detected in the IMC layer. This result explains the bonding strength between the tantalum coating layer and the SUS316L substrate.

Fig. 7 shows the two-dimensional images of the tantalum coating layer formed on SUS316L at different current densities. The surface

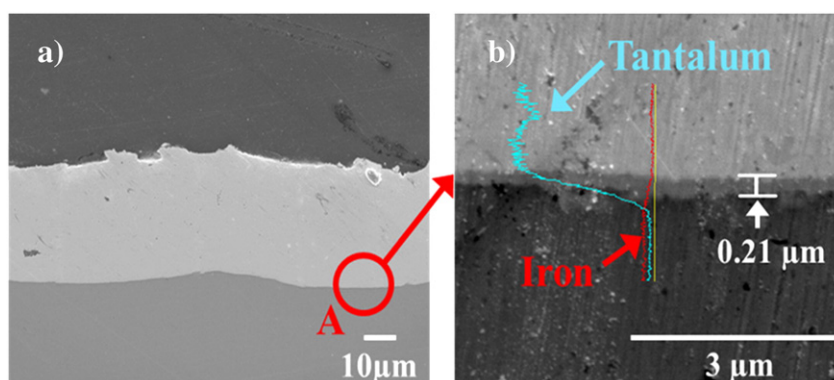


Fig. 6. The cross-section microstructural morphology (a) and composition of IMC layers at the interface (b) between the tantalum-coated layer and SUS316L at 5 mA/cm<sup>2</sup>.

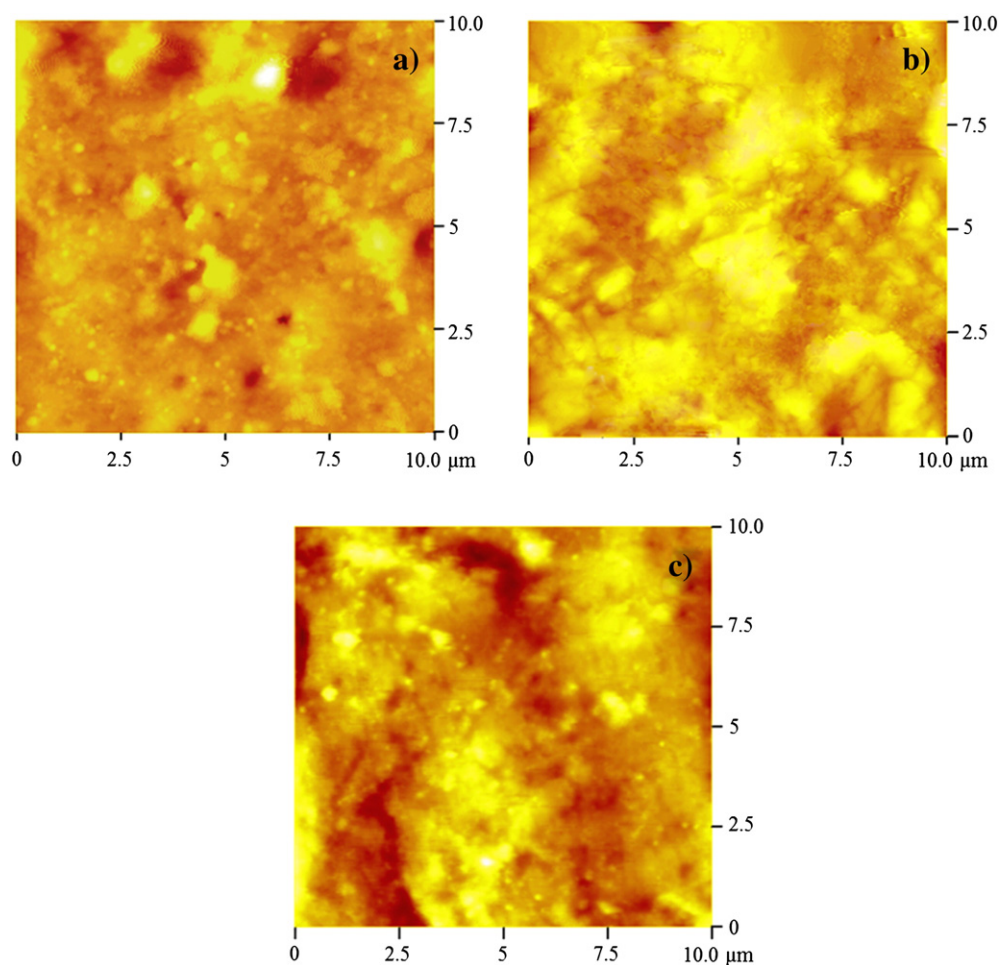


Fig. 7. AFM two-dimensional image map of tantalum coatings at different current densities: a) 1.5 mA/cm<sup>2</sup>; b) 5 mA/cm<sup>2</sup>; c) 20 mA/cm<sup>2</sup>.

roughness (Ra) values of the tantalum coating layers, determined from atomic force microscopy measurements, are shown in Table 3. It was clear that the tantalum coating layer formed at a current density of 1.5 mA/cm<sup>2</sup> has a smoother surface than do the layers coated at 5 mA/cm<sup>2</sup> and 20 mA/cm<sup>2</sup>, indicating that Ra increases with increasing current density.

In order to investigate the effect of the applied current density on the microstructure of the electroplated tantalum coating layer, OIM analyses were carried out to obtain orientation information from the coating layers. Correlation with the surface morphology was achieved by comparing the OIM results with top-view SEM images. The distribution of the crystallographic orientation may be observed in the corresponding OIM map in Fig. 8. Different gray scales indicate the degree of orientations for different tantalum planes. Sub-micrometer-sized tantalum grains were formed at the surface of the SUS316L substrate, and larger grains started to form just after the intermediate layer. The average

grain sizes of the tantalum crystals were 4.85 μm<sup>2</sup> at 1.5 mA/cm<sup>2</sup>, 2.02 μm<sup>2</sup> at 5 mA/cm<sup>2</sup>, and 1.17 μm<sup>2</sup> at 20 mA/cm<sup>2</sup>. In general, according to the pattern presented by Dini [19], the grain size of the deposits is expected to decrease with increasing current density, because an increase in the current density results in a higher overpotential that in turn increases the nucleation rate. The interfacial layer between the substrate and the tantalum layer is already characterized as the IMC layer in Fig. 6(b), and hence, the tantalum coating layer is found to be formed on the IMC layer. In the case of the sample obtained at 20 mA/cm<sup>2</sup>, however, the fine grain layer is not clearly visible as shown in Fig. 8(c). This is because the formation time of the IMC layer is not long enough, owing to the short operational time at a high current density. Moreover, the average grain size drastically decreased from 4.85 μm<sup>2</sup> to 1.17 μm<sup>2</sup> as the current density increased from 1.5 mA/cm<sup>2</sup> to 20 mA/cm<sup>2</sup>.

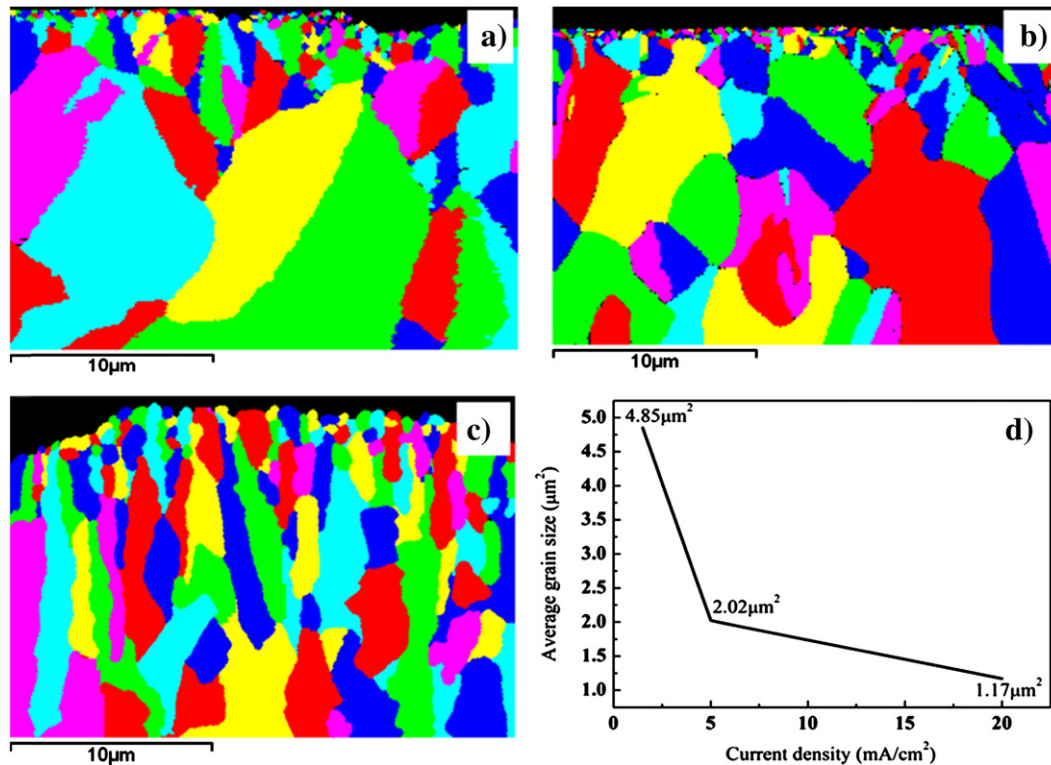
A corrosion test was carried out to measure the corrosion resistance of the tantalum coating layers formed at different current densities, using an autoclave at 160 °C and 20 MPa, in HI (HI = 26.1, I<sub>2</sub> = 51.8,

Table 2  
Corrosion rate at various current densities.

Current density (mA/cm <sup>2</sup> )	Weight before corrosion test (g)	Weight after corrosion test (g)	Corrosion rate (mm/year)
Bare SUS	13.487	0	≥128.210
0.5	14.821	14.623	110.196
1.5	14.821	14.623	0.9334
5	15.078	15.072	0.028
10	14.691	14.012	3.153
20	14.691	14.012	110.241

Table 3  
Surface roughness of tantalum coatings formed at different current densities.

Current density (mA/cm <sup>2</sup> )	Ra (nm)	Rq (nm)	Z range (nm)	Error range (nm)	Scan size (μm)
1.5	23.041	31.759	425.56	79.54	10
5	33.744	43.401	409.89	172.16	10
20	55.891	71.022	578.56	351.48	10



**Fig. 8.** OIM mapping of the cross section of the tantalum coating layer and average grain size change at different current densities: a) 1.5 mA/cm²; b) 5 mA/cm²; c) 20 mA/cm². d) Average grain size change.

H<sub>2</sub>O = 22.0 wt.%) environment. The calculation for the corrosion rate from metal loss is calculated using the following equation:

$$\text{mm/year} = 87.6 \times (W / (D \times A \times T)). \quad (4)$$

In this equation, W represents the weight loss in milligrams, D represents the metal density, A represents the area of the sample, and T represents the exposure time of the metal sample in hours. The corrosion rates of the tantalum coating layers are summarized in Table 2. In the corrosion environment, the bare SUS sample completely dissolved after the corrosion test. In the case of 0.5 mA/cm² and 20 mA/cm² current density, the samples were severely attacked and showed a drastic weight change. The tantalum sample coated at 5 mA/cm² showed the lowest corrosion rate of 0.028 mm/year, while the sample prepared at 20 mA/cm² was severely corroded. The coating layers formed at 0.5 and 20 mA/cm² were not dense enough to be robust to the aggressive high-temperature HI solution.

Fig. 9 shows the microstructural change of the tantalum coating layer after the corrosion test. In the case of 0.5 and 20 mA/cm² current density, it was not possible to analyze the coating layer because most of the substrates were dissolved after the severe corrosion of non-coated SUS. In the case of 1.5 mA/cm² current density, as referred to in Fig. 3, corrosion occurred intensively in the area of bare SUS and the thickness of the coating layer was reduced to  $14.32 \pm 1.71 \mu\text{m}$ . In the case of 5 mA/cm² current density, a difference could be seen when the surface was magnified: the surface was clearly rough in the cross-sectional view shown in Fig. 9b-4). It was certain that the grain boundary was preferentially attacked during the corrosion test, as shown in Fig. 9b-2) and b-3). Hence, the formation of the IMC layer and the coarse microstructure should contribute to better corrosion resistance. These results explain why the specimen obtained at 5 mA/cm² has superior corrosion resistance as compared to the others. In the case of 10 mA/cm² current density, the corrosion occurred intensively in the area of bare SUS, with the porous coating layer falling away during the corrosion test and most of the Ta layer was damaged.

#### 4. Conclusions

Tantalum-coated samples were prepared by electrodeposition in molten salt (LiF–NaF–K<sub>2</sub>TaF<sub>7</sub>) at different current densities. A deposit of pure tantalum was formed on SUS316, and the conclusions are as follows.

- (1) The deposition efficiency and microstructure of the Ta coating layer strongly depended on the current density.
- (2) At a current density of 5 mA/cm², the coating layer thickness ranged from 29.94 µm to 31.31 µm, providing the closest correlation with the designed thickness of 30 µm.
- (3) The grain size of the deposits decreased with increasing current density, because an increase in the current density resulted in a higher overpotential that in turn increased the nucleation rate.
- (4) At a current density of 20 mA/cm², the XRD peaks indicated the presence of the β-Ta phase. This may be the result of an insufficient process time for the transformation to the α-Ta phase.
- (5) The hardness of the tantalum coating layers decreased (331 Hv → 214 Hv) with increasing current density (0.5 mA/cm² → 20 mA/cm²) due to the dendritic growth of a low-density coating layer.
- (6) An IMC layer (thickness: 0.21 µm, concentration: 85.93 wt.% Ta, 14.07 wt.% Fe) formed at the interface between tantalum and the SUS316L substrate. This resulted in an increased bonding strength between the tantalum coating layer and the SUS316L substrate.
- (7) From the results of corrosion tests in HI solution at temperatures up to 160 °C and pressures of 20 MPa, the Ta layer coated at 5 mA/cm² (0.028 mm/year) has a higher corrosion resistance than the Ta layer coated at 1.5 mA/cm² (0.9334 mm/year) and 10 mA/cm² (3.153 mm/year), while the samples prepared at 0.5 mA/cm² (110.196 mm/year), and 20 mA/cm² (110.241 mm/year) were severely corroded.

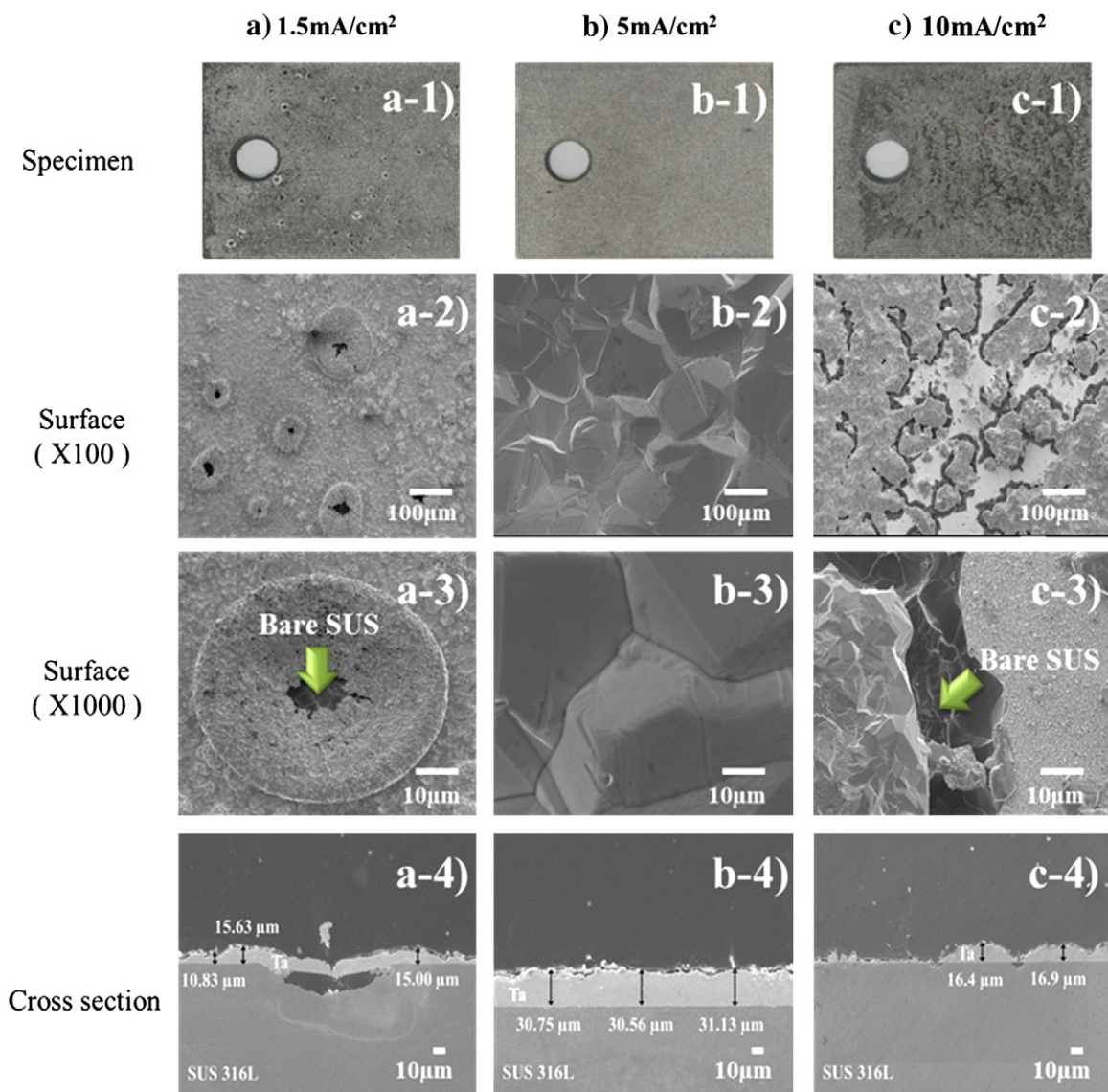


Fig. 9. Microstructures of Ta-coated samples after corrosion test with applied current density: a) 1.5 mA/cm<sup>2</sup>; b) 5 mA/cm<sup>2</sup>; c) 10 mA/cm<sup>2</sup>.

## References

- [1] S. Senderoff, G.W. Mellors, W.J. Reinhart, J. Electrochem. Soc. 112 (1965) 840–845.
- [2] F. Cardarelli, P. Taxil, A. Savall, Int. J. Refract. Met. Hard Mater 14 (1996) 365–381.
- [3] P. Chamelot, P. Taxil, B. Lafage, Electrochim. Acta 39 (1994) 2571–2575.
- [4] I. Ahmad, W.A. Spiak, G.J. Janz, J. Appl. Electrochem. 11 (1981) 291–297.
- [5] P. Taxil, J. Mahenc, J. Appl. Electrochem. 17 (1987) 261–269.
- [6] M. Mehmood, N. Kawaguchi, Y. Sato, T. Yamamura, M. Kawai, K. Kikuchi, Chem. Sustainable Dev. 12 (2004) 99–104.
- [7] M. Mehmood, N. Kawaguchi, H. Maekawa, Y. Sato, T. Yamamura, M. Kawai, K. Kikuchi, Mater. Trans. 44 (2003) 259–267.
- [8] S. Zein El Abedin, H.K. Farag, E.M. Moustafa, U. Welz-Biermann, F. Endres, Phys. Chem. Chem. Phys. 7 (2005) 2333–2339.
- [9] S. Zein El Abedin, U. Welz-Biermann, F. Endres, Electrochem. Commun. 7 (2005) 941–946.
- [10] N. Borisenko, A. Ispas, E. Zschippang, Q. Liu, S. Zein El Abedin, A. Bund, F. Endres, Electrochim. Acta 54 (2009) 1519–1528.
- [11] P. Chamelot, P. Palau, L. Massot, A. Savall, P. Taxil, Electrochim. Acta 47 (2002) 3423–3429.
- [12] A. Girginov, T.Z. Tzvetkoff, M. Bojinov, J. Appl. Electrochem. 25 (1995) 993–1003.
- [13] L.P. Polyakova, E.G. Polyakov, A.I. Sorokin, P.T. Stangrit, J. Appl. Electrochem. 22 (1992) 628–637.
- [14] Z.L. Yuan, D.H. Zhang, C.Y. Li, K. Prasad, C.M. Tan, L.J. Tang, Thin Solid Films 434 (2003) 126–129.
- [15] M.H. Read, C. Altman, Appl. Phys. Lett. 7 (1965) 51–52.
- [16] D.W. Matson, M.D. Mertz, E.D. McClanahan, J. Vac. Sci. Technol. A 10 (1992) 1791–1796.
- [17] S.L. Lee, M. Cipollo, D. Windover, C. Rickard, Surf. Coat. Technol. 120–121 (1999) 44–52.
- [18] S.L. Lee, D. Windover, Surf. Coat. Technol. 108–109 (1998) 65–72.
- [19] J.W. Dini, Electrodeposition: The Materials Science of Coatings and Substrates, Noyes Publications, Park Ridge, NJ, 1993. 141.